An Integrated Computer Supported Acquisition, Handling, and Characterization System for Pigmented Skin Lesions in Dermatological Images

I. Maglogiannis, *Member, IEEE*, S. Pavlopoulos, *Member, IEEE*, and D. Koutsouris, *Senior Member, IEEE*

***Abstract*—This paper describes an integrated prototype computer-based system for the characterization of skin digital images. The first stage includes an image acquisition arrangement designed for capturing skin images, under reproducible conditions. The system processes the captured images and performs unsupervised image segmentation and image registration utilizing an efficient algorithm based on the log-polar transform of the images' Fourier spectrum. Border- and color-based features, extracted from the digital images of skin lesions, were used to construct a classification module for the recognition of malignant melanoma versus dysplastic nevus. Different methods, drawn from the fields of artificial intelligence (neural networks) and statistical modeling (discriminant analysis), were used in order to find the best classification rules and to compare the results of different approaches to the problem.**

***Index Terms*—Classification, image analysis, registration, segmentation, skin lesion.**

I. Introduction

MEDICAL professionals in dermatology base the diagnosis of skin lesions mainly on the visual assessment of pathological skin and the evaluation of macroscopic features. This fact shows that correct diagnosis is highly dependent on the observer's experience and on his or her visual perception. Moreover, the human vision lacks accuracy, reproducibility, and quantification in the way it gathers information from an image. In addition, a significant amount of studies have proven that the quantification of tissue lesion features may be of essential importance in clinical practice, because several tissue lesions can be identified based on measurable features extracted from a digital image [1], [2], [5], [7], [8], [11], [13], [18], [19], [41]. In addition, the use of digital image features may help in an objective follow-up study of skin lesion progression and test the efficacy of therapeutic procedures. The present paper describes the implementation of an integrated prototype for a computer-based image analysis system, intended for the characterization of dermatological images and particularly for the recognition of malignant melanoma versus dysplastic nevus. The innovative elements of the system are: its ability to acquire repeatable and high-quality images, as regards color and resolution, the standardization of the acquisition procedure and the integration of discrete software modules performing unsupervised segmentation, registration, and classification into a single system.

The paper is organized as follows. In Section II, we describe the imaging system we implemented for the acquisition of reproducible skin images. Section III provides a comparative study of six methodologies for the segmentation and contour extraction of the pigmented skin lesion. Section IV presents an efficient algorithm based on the log-polar transform of the images' Fourier spectrum for achieving registration during follow-up studies, which was applied on images acquired by our system. In Section V, we describe the feature extraction and we give background information for the method of discriminant analysis and the neural network model incorporated for the lesion assessment. In Sections VI and VII, we provide the results of the classification procedure, and finally in Section VIII, we conclude the paper. The complete architecture of the implemented image analysis system as a whole is depicted in Fig. 1.

II. Image Acquisition

The first step in such an image analysis system intended for characterization of skin lesions involves the acquisition of the tissue digital image. Probably the most important problem, which has to be resolved concerning the design and implementation of the acquisition system, is its ability to capture reliable and reproducible images. The reproducibility is considered essential for image analysis classification and for the comparison of sequential images during follow-up studies. However, the acquisition of reproducible images is quite challenging due to equipment and environmental constraints, such as image resolution, image noise, illumination, skin reflectivity, and poses uncertainty.

The use of commercially available photographic cameras is quite common in skin lesion inspection systems, particularly for telemedicine purposes [15]. However, the relatively poor resolution in very small skin lesions (i.e., lesions with 0.5-cm diameter) and the fact that variable illumination conditions are not easily handled, make these devices insufficient for capturing skin lesions with high requirements in resolution and color measurement. The first problem may be solved if appropriate lenses with small focal length are placed in front of the cameras. Furthermore, new models with better resolution capabilities are expected in the near future. The second problem, though

Manuscript received May 31, 2003; revised October 15, 2003 and February 24, 2004.

I. Maglogiannis is with the Department of Information and Communication Systems Engineering, University of Aegean, 83200 Karlovasi, Samos, Greece (e-mail: imaglo@aegean.gr).

S. Pavlopoulos and D. Koutsouris are with the Department of Electrical and Computer Engineering, Biomedical Engineering Laboratory, National Technical University of Athens, 15773 Zografou Campus, Athens, Greece (e-mail: spav@biomed.ntua.gr; dkoutsou@biomed.ntua.gr).

Digital Object Identifier 10.1109/TITB.2004.837859

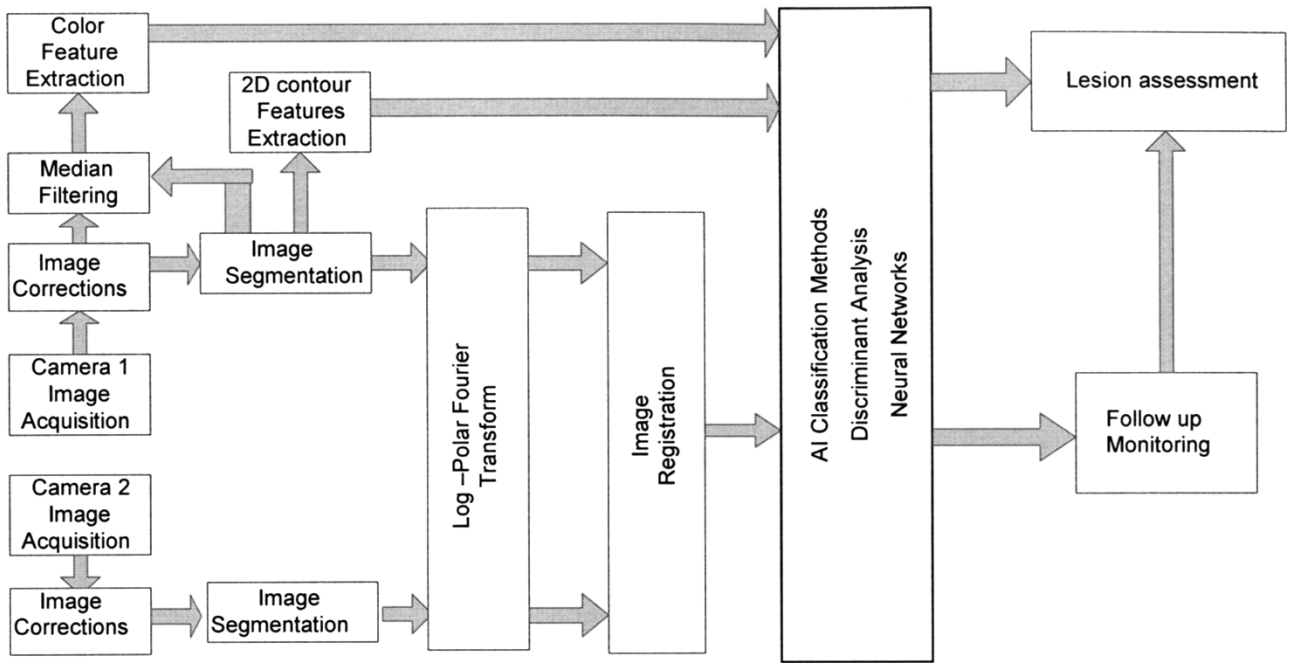

Fig. 1. Schematic representation of the complete digital image analysis architecture implemented in our system.

considered necessary for the reproducibility of the images, is a rather complex, difficult, and sensitive task, as it requires automated color calibration of the camera. Color calibration refers to the adjustments and corrections that are necessary to allow the camera to work within its dynamic range and measure always the same color regardless of the lighting conditions of the skin lesion or the surrounding environment. The problem can be solved to some extend by using video cameras that are configurable online and can be easily controlled through software [42].

The image noise is mainly attributed to the limitations of the image acquisition hardware (sensor elements, digitizer) and the finite spatial resolution of the charged-coupled device (CCD) chips. Crosstalking between neighboring pixels is also a factor that contributes to noise. Particles of variable geometric characteristics on the skin, such as hair, dust, etc., cause additional problems to the reproducibility of the acquired images. Noise can be eliminated through appropriate filtering, e.g., morphological filtering to preserve edge information [27] or median filtering to assist color identification [17].

The scene illumination is probably the most influential factor on lesion inspection. Nonconstant scene illumination may lead to totally different and, thus, nonreproducible images. Therefore, engineering of the environment is applied to ensure invariable illumination. Moreover, a major problem in digital skin image acquisition involves the reflections of the incident light. The human skin, because of its irregular surface, scatters incident light in irregular directions, burying diagnostic information. A complete solution to the image acquisition problem should use appropriate lighting geometry to reduce the light reflections and software corrections that are applied to the image during the acquisition. To optimize color rendering ability, lamp temperature should be within the 2900 K–3300 K range, with a color rendering index (degree of ability to produce light

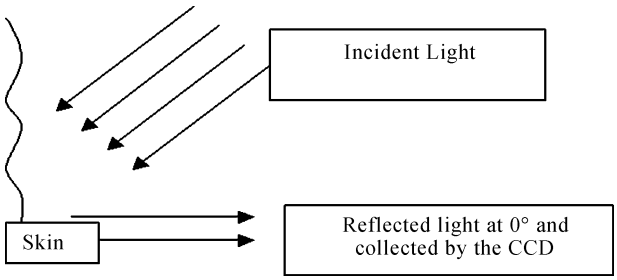

Fig. 2. Partial reflection at 0° due to the curved surface of the skin.

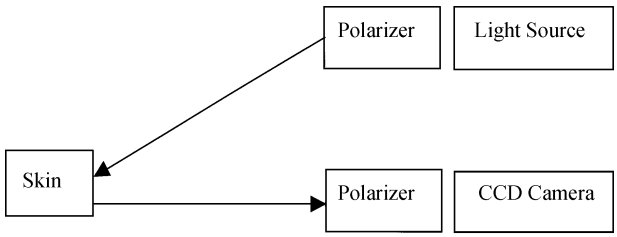

Fig. 3. Polarizing filter transmits only the component of the oscillation that is directed in the polarizing direction of the filter. The angle between the directions of the two polarizers is set to 90° to eliminate light reflections.

output optimal for true color rendering) of 85 or higher [21], [22]. The light of the lamp should be transmitted and delivered onto the surface at an angle of 45° and the reflected light should be collected at 0° to the surface normal. This illumination and capturing geometry is internationally established for color measurements, because it eliminates shadows and reflections [54]. However, it is very difficult to create uniform illumination at an angle greater than 45° over the entire field of view and over curved surfaces as it is depicted in Fig. 2. Therefore, in our image acquisition system, polarizing filters were also used for eliminating the remaining reflections (Figs. 3 and 4).

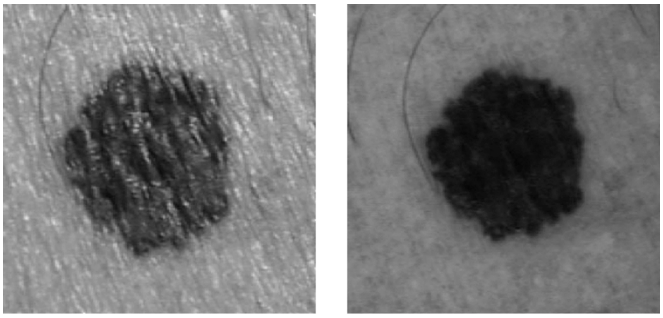

(a) (b)

Fig. 4. Skin lesion image acquired with polarizing filters (a) in parallel relative position and (b) in vertical relative position. In the second case, the reflections are significantly reduced.

With regard to the software corrections, three main types were implemented: color calibration incorporating the Gretag–McBeth Color Calibration chart,[1] shading correction, and median filtering. Shading correction is performed by a division pixel-by-pixel of an image with all pixels having $R = G = B = 255$ by the image of a perfect diffuser ($BaSO_4$) and then multiplying a captured image with the look-up table generated by the division [54]. Median filtering was also used in [17] and [18] for removing noise from skin digital images. In our study, we tried Median filtering and a simple 3×3 weighted averaging mask and we saw that Median filtering has a slightly better effect on the segmentation performance. Noise removal due to dark hairs may be improved if more sophisticated algorithms are adopted. Such an algorithm is presented in [20]. The specific technique relies on identifying the hair location by utilizing morphological operators and replacing the hair pixels by the nearby nonhair pixels.

The utilized image acquisition system illustrated in Fig. 5 consists of the following:

- a typical 3-chip CCD microhead color video camera (Panasonic GP-US502) with resolution 811(H) $\times$ 508(V) pixels in visible spectra and a red-green-blue (RGB) output;
- a 150-W 21-V quartz halogen lamp, with color temperature of 3300 K with relatively smooth spectrum without many spikes;
- a personal computer;
- circular polarizing filters in front of the CCD receiver and the light focusing lens.

In order to assess the validity of the calibration procedure and the ability of the implemented image acquisition subsystem to produce reproducible images, we captured ten series of sample images in three different lighting conditions of the surrounding environment: dark, medium, and intense lighting. For each series, we captured a skin lesion in medium lighting environmental conditions, we segmented it, and we calculated the average values of the three-color planes RGB and their standard deviations. These values were used as reference. Then we changed the surrounding lighting conditions, we performed calibration, and we recaptured the same skin lesion. After its segmentation, we calculated again the average values and their deviations and we compared them with the reference values. The measured error differences ranged between 0.4 and 13.2 (in the 0–255 scale) for the average RGB values and 1.6 and 17.9 for their standard deviation. The corresponding mean errors were 7.8 and 12.3 or $7.8/255 = 3.05\%$ and $12.3/255 = 4.82\%$. The above measurements concern only the color features of the captured images and they are also depicted in Table I.

Experimental results demonstrate the reproducibility of the captured images at a satisfactory level. The remaining aberration is electronic noise caused by the CCD. A typical technique to eliminate this kind of noise, which is stochastic with zero mean value, is averaging sequential captured images of the same object. Unfortunately, in our case, the minor movements of the patient during the image acquisition prevented us from using this technique.

[1]GretagMacbeth Corporation. [Online]. Available: http://www.gretagmacbeth.com.

III. Image Segmentation

The segmentation of an image containing a cutaneous disease involves the separation of the skin lesion from the healthy skin. For the special problem of skin lesion segmentation, mainly region-based segmentation methods are applied [39], [40], [43]. The following segmentation algorithms were utilized and compared in the developed system.

A) *Thresholding*, which is based on the fact that the values of pixels that belong to a skin lesion differ from the values of the background. By choosing an upper and a lower value, it is possible to isolate those pixels that have values within this range. The information for the upper and the lower limits can be extracted from the image histogram, where the different objects are represented as peaks. The bounds of the peeks are good estimates of these limits [Fig. 6(a)]. It should be noted though that simple thresholding as it is described here cannot be used in all cases because image histograms of skin lesions are not always multimodal.

B) *The use of weighted functions* [Fig. 6(b)] presupposes that two small windows, one inside and one outside the skin lesion area, are identified in order to calculate the weight vector. The two small windows can be identified using approximate segmentation strategy or by human intervention. Then typical values of the three-color planes are computed for the two windows and a function is formed where the contribution of each color plane is defined by the size of variation between the two windows. A simple approach uses the average values of the two windows.

C) *Region growing* [Fig. 6(c)] is a procedure that groups pixels or subregions into larger regions [24]. In skin lesion images where the color differences are intense, this technique has excellent results. The major advantage is that it allows small alterations of the skin lesion and that it ends in compact boundaries.

D) In the *principal components transform* (PCT) [Fig. 6(d)] method, the eigenvectors of the covariance matrix are calculated and they are used as a linear transformation matrix on the original (RGB) values.

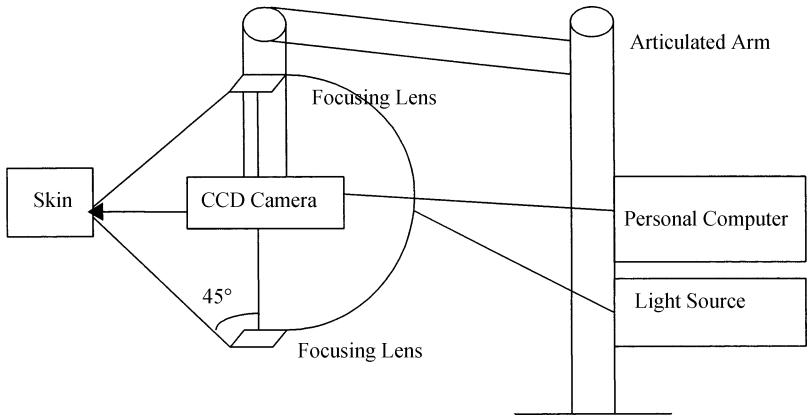

Fig. 5. Lighting geometry of the image acquisition system consists of a color video camera, two focusing lenses (mounted on an articulated arm) that face the target at an angle of 45°, a light source that sends lights to the lenses through fiber optics, and a personal computer for image processing.

TABLE I
MEASURED ERROR DIFFERENCES IN RGB COLOR PLANE BETWEEN THE THREE DIFFERENT LIGHTING CONDITIONS

Type	Measured Differences	
	Absolute (in the 0-255 scale)	Percentage (%)
Maximum Difference for Mean Value	13.2	5.18
Maximum Difference for Standard Deviation	17.9	7.02
Mean Difference for Mean Value	7.8	3.05
Mean Difference for Standard Deviation	12.3	4.82

This method, described in [53], ends in uncorrelated vectors. This can be seen geometrically as an alignment of the primary axis, so that the variance in the data is maximal. In order to find the PCT for a given image, the covariance matrix must first be found. The three-dimensional covariance matrix of a color image is defined as follows:

$$\mathrm{COV} = \begin{bmatrix} C_{\mathrm{RR}} & C_{\mathrm{GR}} & C_{\mathrm{BR}} \\ C_{\mathrm{RG}} & C_{\mathrm{GG}} & C_{\mathrm{BG}} \\ C_{\mathrm{RB}} & C_{\mathrm{GB}} & C_{\mathrm{BB}} \end{bmatrix} \tag{1}$$

where

$$C_{XX} = \frac{1}{N}\sum_{i=1}^{N}(X_i - \mu_X)^2$$

$$C_{XY} = C_{YX} = \frac{1}{N}\left[\sum_{i=1}^{N} X_i Y_i\right] - \mu_X \mu_Y$$

$$\mu_X = \frac{1}{N}\sum_{i=1}^{N} X_i$$

and

$$X, Y \in \{R, G, B\}.$$

The vectors in the new space $[X_1\ X_2\ X_3]^T$ are obtained by

$$\begin{bmatrix} X_1 \\ X_2 \\ X_3 \end{bmatrix} = \begin{bmatrix} E_{11} & E_{12} & E_{13} \\ E_{21} & E_{22} & E_{23} \\ E_{31} & E_{32} & E_{33} \end{bmatrix} \begin{bmatrix} R \\ G \\ B \end{bmatrix} \tag{2}$$

where $[E_{11}\ E_{12}\ E_{13}]$, $[E_{21}\ E_{22}\ E_{23}]$, and $[E_{31}\ E_{32}\ E_{33}]$ are the eigenvectors of the covariance matrix.

It has been experimentally determined in [50] that in the case of skin tumor images, the axis with the largest variance after the appliance of PCT contained approximately 91% of the total variance. This axis may be used for the division of the image into the desired number of segments. An estimation of the X_1 values for the lesion and the healthy image may be obtained from windows inside and outside the skin lesion area. Then the Euclidean distance measure is used to map each pixel to the closest class segment.

E) The CIELAB color space transform is effective in measuring chromatic differences between pixels [24]. An estimate of the color of the background is obtained from small windows in the corners and the color difference is calculated for all pixels producing the color difference image. This image is smoothed by a low-pass filter, edge detected with Sobel operator, and the image segmentation is performed by defining a threshold value for the intensity of the edge detected image [see Fig. 6(e)].

F) The spherical coordinates transform [Fig. 6(f)] was introduced in [25] for the identification of color variegation in dermatological images. The transformation converts the Cartesian RGB Space into a spherical domain, where the pixel color is represented by two color angles, and a one-dimensional intensity space. The transform equations are as follows:

$$L = \sqrt{R^2 + G^2 + B^2} \tag{3}$$

$$\mathrm{Angle}A = \cos^{-1}\left[\frac{B}{L}\right] \tag{4}$$

$$\mathrm{Angle}B = \cos^{-1}\left[\frac{R}{L\sin(\mathrm{Angle}A)}\right]. \tag{5}$$

The two color angles A and B were used then for segmenting the image.

Fig. 6 displays examples of skin lesions segmentation using the above algorithms. In order to determine the success of the computer-calculated border relative to the true border, we asked

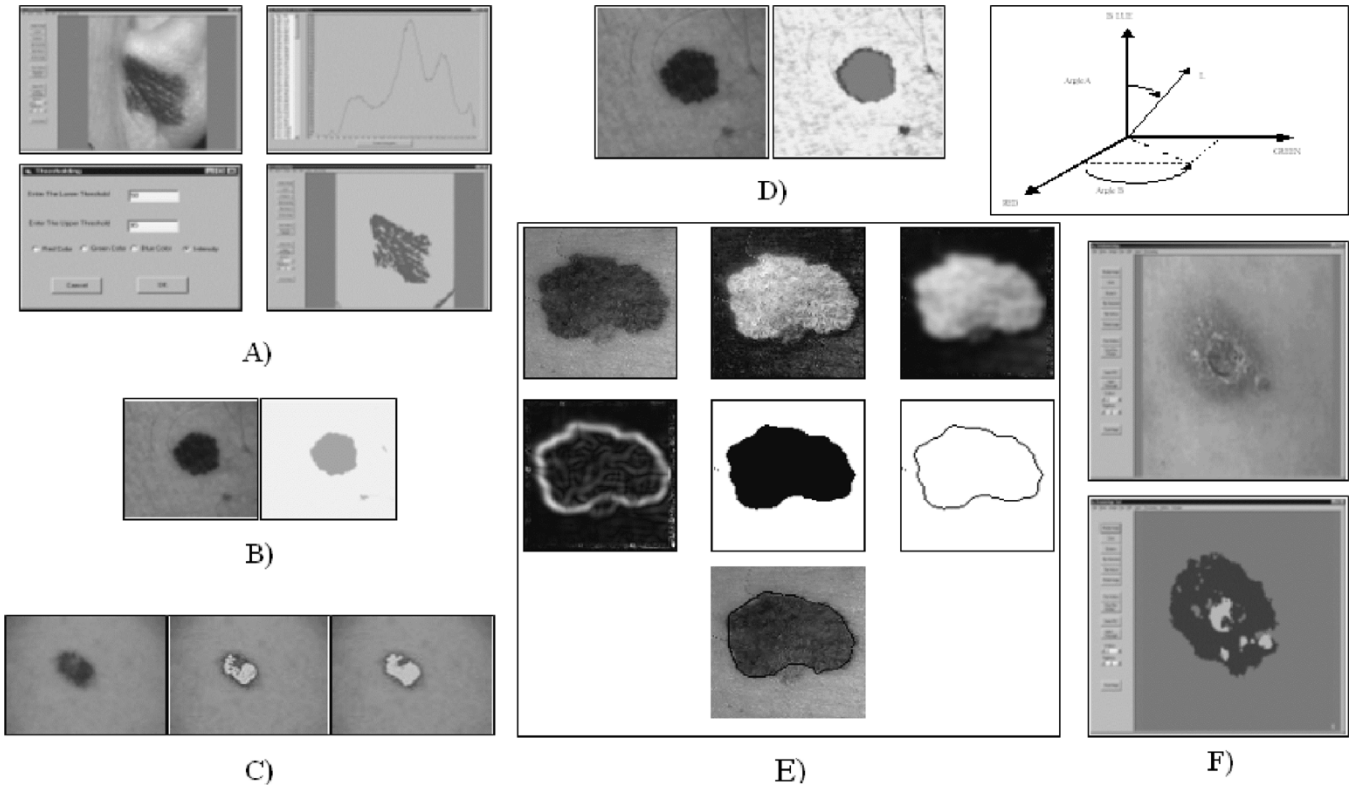

Fig. 6. Examples of image segmentation using the six algorithms implemented. (a) Thresholding. (b) Use of weighted function. (c) Region growing. (d) PCT transform. (e) CIELAB color space. (f) Spherical coordinate transform.

TABLE II
MEASURE OF PERFORMANCE OF THE SEGMENTATION ALGORITHMS

Algorithm	Common Pixels between the two the two segmentations (%)	Pixels that belong to the computer-based segmentation and not to the manually determined (%)	Pixels that belong to the manually determined segmentation and not to the computer-based (%)
Thresholding	60.29	19.16	20.59
Weighted Function	79.51	7.03	13.49
Region Growing	69.12	22.86	8.02
PCT Transform	83.62	7.50	9.09
CIELAB Color Space	73.50	16.41	3.94
Spherical Coordinates	79.19	9.86	10.95

an expert dermatologist to draw manually the border on the digital image. The metric used for the performance of the segmentation algorithms was the percentage of common pixels between the two areas defined by the two borders, calculated as the ratio of the intersection divided by their union. We have also calculated the percentage of pixels that belong to the computer-based lesion and not to the manually determined lesion and vice-versa. Segmentation algorithms tests included 50 digital images and the results are displayed in Table II. It should be noted though that manual outlining suffers from low interoperator and intraoperator agreement and the results could be different if another physician was selected. At the same time, it is very difficult to get the outlines from many operators; however, Table II gives an indication of each algorithm performance.

IV. IMAGE REGISTRATION

Image registration is a procedure of finding correspondence between two different images in order to correct transpositions and scaling caused by changes in camera position. This procedure is necessary for monitoring the progress and measuring the changes of skin lesions. Image registration allows the computation of border-based features, which may be used as objective indexes for the progress of skin tumors and of therapeutic procedures.

The input of an image registration algorithm consists of the two images and the output is the values of four parameters: magnification, rotation, horizontal shifting, and vertical shifting [26]. The implementation involves the selection of a similarity criterion, which measures the similarity of the two images. The most commonly used criteria are the correlation coefficient [27], the correlation function, and the sum of the absolute values of the pixel differences. The second step is an optimization algorithm, which maximizes the similarity criterion. The complexity of the problem (at least four independent parameters) makes the use of exhaustive algorithms ineffective. The use of random search algorithms is a generally acceptable technique for the optimization of nonlinear problems. Their major advantage is easy implementation. On the other hand, though, their efficiency is based on probability factors and their behavior is not predictable.

A lot of algorithms have been proposed for the solution of the medical image registration problem. According to a classification made in [47], the most common approaches are the 1) landmark-based, 2) segmentation-based, 3) voxel property-based, and 4) transformation-based registration methods. Landmark-based algorithms require the selection of a number of corresponding landmarks; landmarks are anatomical, i.e., salient and accurately locatable points of the morphology of the visible skin anatomy, usually identified interactively by the user and secondly by the utilization of an interpolating transformation model, i.e., thin-plate splines [48]. Segmentation-based methods rely on prior image data reduction achieved by segmentation and voxel property-based algorithms rely on the correlation between original images or extracted feature images or the maximization of mutual information (relative entropy) of properties, such us the image histogram [49]. In order to overcome the complexity of the problem, we introduce an effective unsupervised deterministic and transformation-based algorithm that uses the cross-correlation of the log-polar Fourier spectrum [28]. The Fourier transformation spectrum is independent of horizontal and vertical shifting, while the use of the log-polar transform eliminates the dependency on magnification and rotation. If the two images are $f(x,y)$ and $f'(x,y)$, they are connected through a four-parameter geometric transformation, which is described by the following:

$$f'(x,y) = f\left(a(x\cos b + y\sin b) - \Delta x,\ a(-x\sin b + y\cos b) - \Delta y\right) \quad (6)$$

where Δx and Δy are the parallel shifting, a is the magnification factor, and b is the rotation angle. The Fourier spectra of the two images are connected by the following:

$$|F'(u,v)| = \frac{1}{a^2}\left|F\left(\frac{(u\cos b + v\sin b)}{a}, \frac{(-u\sin b + v\cos b}{a}\right)\right| \quad (7)$$

which displays the independence of horizontal and vertical shifting. Then the log-polar transformation is performed

$$|F'(r,\theta)| = \frac{1}{a^2}\left|F\left(\frac{r}{a}, \theta + b\right)\right| \quad (8)$$

where

$$r = \sqrt{u^2+v^2}, \quad \theta = \tan^{-1}\frac{v}{u} \quad (9)$$

and

$$|F'(\rho,\theta)| = \frac{1}{a^2}\left|F\left(\rho - \ln(a), \theta + b\right)\right| \quad (10)$$

where

$$\rho = \ln(r). \quad (11)$$

This mapping of the Fourier magnitudes into polar coordinates (r,θ) achieves the decoupling of the rotation and scale factors; rotation maps to a cyclic shift on the θ-axis and scaling maps to a scaling of the r axis. A logarithmic transformation of the r axis further transforms scaling into a shift. The next step is the use of the cross-correlation function to find the scale factor and the rotation angle that maximizes the corresponding criterion

$$XC(R,T) = \sum_{\rho=\rho_{\min}}^{\rho_{\max}} \sum_{\theta=0}^{2\pi} F(\rho+R, \theta+T)F'(\rho,\theta) \quad (12)$$

where the parameters are the log-difference of the scale factors R and the difference of the rotation angle T. The problem is then reduced to finding the horizontal and vertical shifting, which is simpler, and we resolved it using classical the comparison method of the sum of the absolute values of the differences. An example of the registration procedure is provided in Fig. 7.

The results showed that log-polar Fourier transform had good performance in measuring small rotations up to 10°. For larger rotations, the algorithm had a tendency to calculate greater rotation values than the real ones. Regarding the calculation of the scale factor, the algorithm had better accuracy for values below 1.0, thus, for image scale down. Fig. 8(a) and (b) shows results produced by applying the log-polar Fourier algorithm for a number of manually specified rotation and magnification values. The bulleted curves correspond to the measured rotation and magnification, while the line represents the correct values.

V. Feature Extraction and Classification Methods

In automated diagnosis of skin lesions, feature design is based on the so-called ABCD-rule of dermatology. The ABCD rule, which constitutes the basis for a diagnosis by a dermatologist [45] represents the asymmetry, border structure, variegated color, and the diameter of the skin lesion.

The feature extraction is performed by measurements on the pixels that represent a segmented object allowing non-visible features to be computed. Several studies have proven the efficiency of border shape descriptors for the detection of malignant melanoma on both clinical and computer-based evaluation methods [10]. In our study, the border-based features computed are Greatest Diameter, Area, Border Irregularity, Thinness Ratio, and Border Asymmetry, defined as follows.

Irregularity is defined as

$$\text{Irregularity } A = \frac{\text{Perimeter}}{\text{Area}}. \quad (13)$$

This ratio depends on the size of the skin lesion, therefore, the calculation of the irregularity is more correct as the ratio

$$\text{Irregularity } B = \frac{\text{Perimeter}}{\text{Greatest Diameter}}. \quad (14)$$

Thinness Ratio measures the circularity of the skin lesion. It is defined as

$$\text{ThinessRatio} = 4\pi\frac{\text{Area}}{(\text{Perimeter})^2}. \quad (15)$$

This measure has a maximum value of one, which corresponds to a circle. It can be used for the detection of skin diseases, which have the property to spread radial on the human skin. Finally, border asymmetry is computed as the percent of nonoverlapping area after a hypothetical folding of the border around the greatest diameter [44].

For the calculation of the above border-based features, actual geometrical dimensions were used. A small scale was placed by

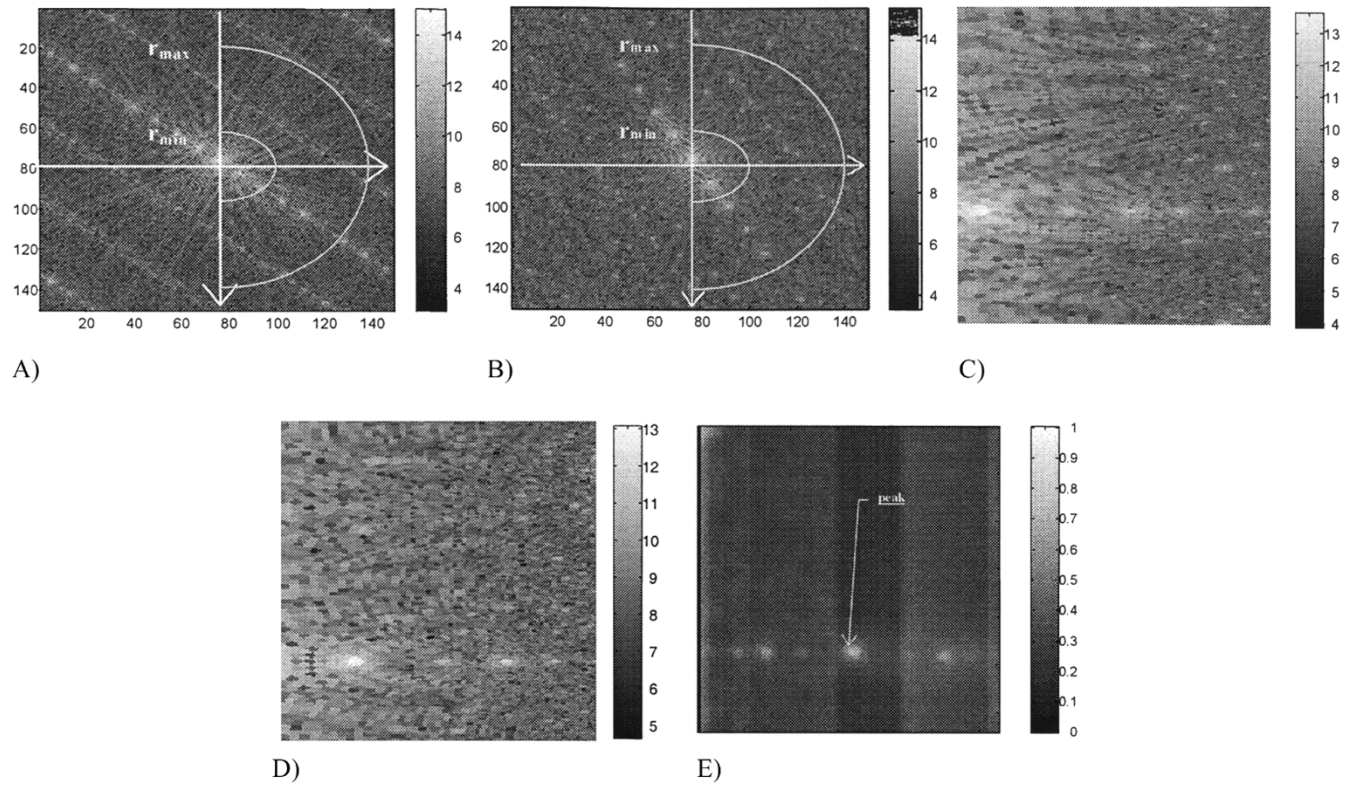

Fig. 7. Example of the image registration procedure. (a) Fourier spectrum of a dermatologiacal image. (b) Fourier spectrum of the same image rotated by 20° and scaled down by a factor 0.8. (c) log-polar transform of image A. (d) log-polar transform of image B (NB: Magnification and rotation have been transformed to horizontal and vertical shifting). (e) Application of the cross-correlation coefficient to find the scale factor and the rotation angle.

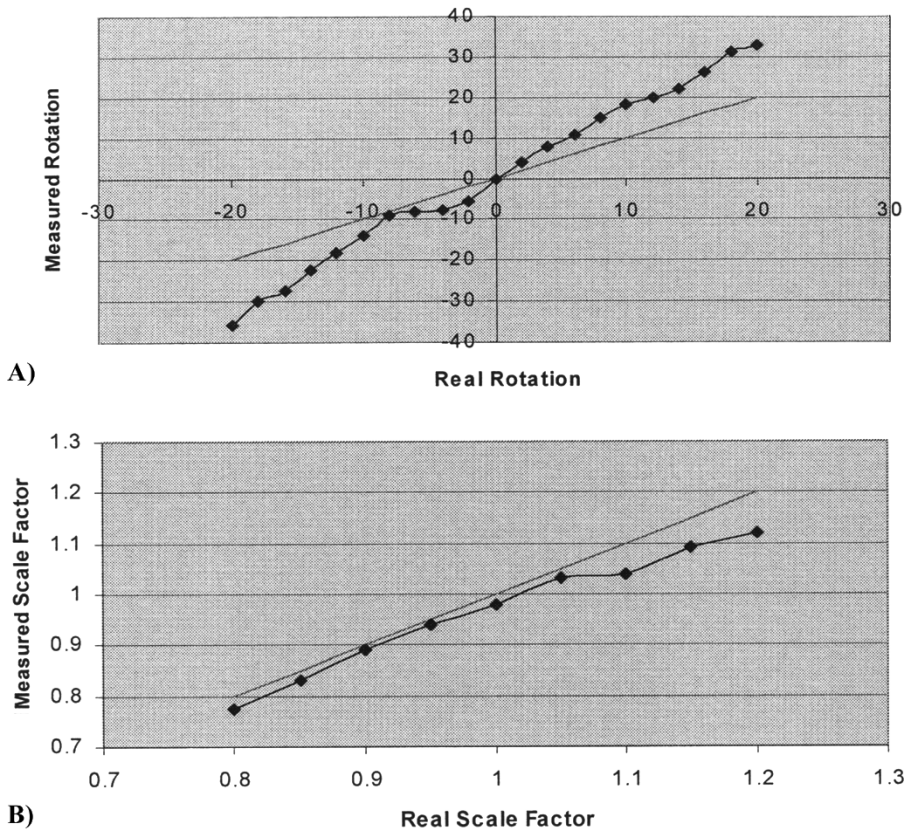

Fig. 8. Accuracy of the log-polar Fourier transform in (a) the calculation of the rotation and (b) scale factor.

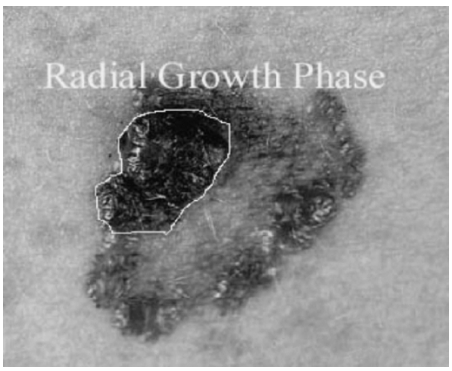

Fig. 9. RGP phase of melanoma is the circled area.

the side of each lesion and was also captured in the image. Then, in each image, the proportion of image pixels with physical dimensions was calculated and afterwards the scale was cropped.

The second feature category involves the actual values of the pixels that are located inside the border and, thus, correspond to the skin lesion. The color features incorporated in the classification module are mainly statistical parameters calculated from different color channels. More specifically, they are based on measurements on the RGB and the hue, intensity, and saturation (HIS) color planes and the transformation to spherical coordinates LAB. Color variegation was also calculated by measuring standard deviations of the RGB channels and chromatic differences inside the border [41]. Finally, a heuristic linear transformation presented in [29] and [30] was also incorporated as follows:

$$I_1 = \frac{(R+G+B)}{3} \tag{16}$$

$$I_2 = (R-B) \tag{17}$$

$$I_3 = \frac{(2G-R-B)}{2}. \tag{18}$$

The basic aim is to construct a classification system for skin lesions, enabling the distinction of malignant melanoma from dysplastic nevus. Three groups of data will be considered. The first group (denoted VGP) consists of 14 cases of malignant melanoma, with measurements taken on the entire extent of the lesion. The second group (RGP) also refers to the malignant melanomas, but measurements are restricted to the dark area of the melanoma. The third group (DSP) comprises 20 cases of dysplastic nevus (see Fig. 9).

Regarding the statistics of the lesions, the mean diameters were 0.84 and 1.56 cm for dysplastic naevi and melanomas, respectively. The mean thickness of melanoma lesions was measured during biopsy at about 1.5-mm penetration through the skin. Mean values of each variable in each group are shown in Table III. Separate analyses were carried out, one between VGP and DSP, and the other between RGP and DSP. Both comparisons were made by linear discriminant analysis and also by fitting a neural network model.

Several machine learning methods may be incorporated for the classification of the three aforementioned classes [38]. In our system, we chose to implement two different approaches, one drawn from statistical modeling (discriminant analysis) and one from the field of artificial intelligence (neural networks), and compare the results.

TABLE III
MEAN VALUES (STANDARD DEVIATIONS IN PARENTHESES) OF FEATURES, BY GROUP

Features	DSP	RGP	VGP
Irregularity A	0.058 (0.028)	0.030 (0.016)	0.041 (0.016)
Irregularity B	3.38 (0.20)	3.06 (0.56)	4.05 (0.47)
Thinness Ratio	0.66 (0.04)	0.98 (0.35)	0.48 (0.10)
Red (Average)	69.5 (10.6)	36.3 (19.6)	104.5 (48.8)
Green (Average)	66.1 (19.4)	36.5 (8.4)	78.5 (31.3)
Blue (Average)	49.5 (18.3)	28.1 (9.7)	67.2 (33.0)
Red (St.Dev.)	22.1 (10.8)	18.3 (7.9)	37.4 (14.0)
Green (St.Dev.)	23.3 (8.9)	16.5 (6.0)	30.2 (12.7)
Blue (St.Dev.)	21.3 (8.1)	16.2 (5.5)	29.3 (12.3)
I_1 (R+G+B / 3)	62.8 (9.9)	33.6 (15.6)	92.0 (43.0)
I_2 (R-B)	20.0 (19.9)	8.3 (14.0)	37.3 (21.4)
I_3 (2G-R-B /2)	6.61 (11.34)	4.25 (6.85)	-7.36 (11.22)
Average Intensity	62.8 (13.4)	33.6 (11.8)	83.4 (37.1)
Average Hue	1.23 (0.83)	1.66 (0.84)	1.08 (0.75)
Average Saturation	0.27 (0.13)	0.30 (0.11)	0.24 (0.13)
Average L	109.8 (21.7)	60.0 (20.9)	148.3 (65.6)
Average Angle A	1.13 (0.11)	1.09 (0.10)	1.12 (0.09)
Average Angle B	0.74 (0.17)	0.87 (0.22)	0.67 (0.08)
Greatest Diameter	84.1 (28.9)	156.3 (50.0)	279.8 (90.4)
Asymmetry	13.5 (11.1)	10.9 (4.1)	26.2 (10.3)

The main aim of discriminant analysis [31] is to allocate an individual to one of two or more known groups, based on the values of certain measurements $\mathbf{x}$. The discriminant analysis procedure identifies the combination of these predictor variables that best characterizes the differences between groups. The procedure estimates the coefficients, and the resulting discriminant function can be used to classify cases. The analysis can also be used to determine which elements of the vector of measurements $\mathbf{x}$ are most useful for discriminating between groups. This is usually done by implementing stepwise algorithms, as in multiple regression analysis, either by successively eliminating those predictor variables that do not contribute significantly to the discrimination between groups, or by successively identifying the predictor variables that do contribute significantly.

One important discriminant rule is based on the likelihood function. Another important approach is Fisher's Linear Discriminant Function [31]. Preliminary data exploration by constructing normal probability plots for each variable in each group separately indicated that most variables measured in this study followed distributions that were reasonably close to the normal distribution. It was, therefore, decided to apply discriminant analysis to the data as they stood, and to defer further investigation of possible transformations of variables to a later time when more cases would be available for analysis.

The methodology of neural networks involves mapping a large number of inputs into a small number of outputs and it is, therefore, frequently applied to classification problems [32] in which the predictors $\mathbf{x}$ form the inputs and a set of variables denoting group membership represent the outputs. It is, thus, a major alternative to discriminant analysis, and therefore, a comparison between the results of these two entirely different approaches is interesting. Neural networks are very flexible as they can handle problems for which little is known about the form of the relationships.

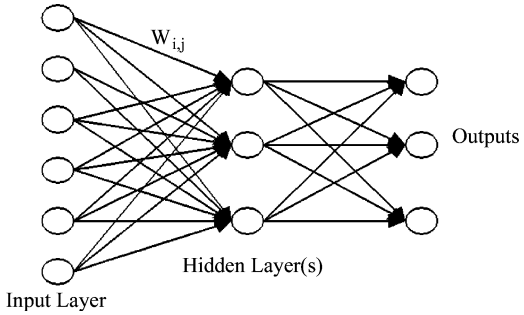

Fig. 10. Generic feed-forward neural network used for classification.

In the basic feed-forward neural network, an input layer sends signals to a hidden middle layer, as in Fig. 10. The hidden layers can be thought of as a form of intermediate processing of the data. One hidden layer will normally suffice for classification problems [33].

Feed-forward neural networks with one hidden layer and allowing skip-layer connections directly from the input to the output nodes were fitted in this study using the S-Plus programming language. Because of the excessively large number of input variables available, and the lack of any automated procedure for variable selection, it was decided to reduce the number of inputs to the neural network models by taking principal components of the 20 variables and alternatively by using the variable combinations that had been selected in the corresponding discriminant analyses. Principal components analysis is the most common method of reducing the dimensionality of multivariate statistical data [31]. However, as indicated earlier in Section III, it uses a variance maximization criterion and this is not necessarily relevant to discrimination. Therefore, other model selection criteria will be applied at a later stage of this work.

VI. VGP-DSP Comparison

Preliminary comparisons for each variable separately, using simple t tests, indicated that 7 of the 20 variables differed statistically significantly $(P < 0.01)$ between the two groups. These were: Irregularity, Thinness Ratio, Average Red, Standard Deviation of Red, I_3, Greatest Diameter, and Asymmetry. A stepwise discriminant analysis (carried out using the SPSS package) using forward selection of significant predictors (with the criterion of Wilks' lambda statistic, indicating the separation between the groups in the multivariate space) selected the Greatest Diameter and the Thinness Ratio as the most significant for discrimination. The diagnosis of malignant melanoma was indicated by higher values of the Greatest Diameter (mean 280 in VGP cases, 84 in DSP) and by lower values of the Thinness Ratio (means 0.48 and 0.66 for VGP and DSP, respectively). Feature selection may be also dealt by more sophisticated algorithms such as sequential forward floating selection or generalized sequential forward selection presented in [52].

This discriminant function classified correctly 97% of cases (93% of VGP and 100% of DSP). This is the cross-validation or "leaving-one-out" estimator of the rate of correct classifications, obtained by seeing how each observation is classified according to a discriminant function recalculated after omitting that observation from the analysis. The cross validation procedure was basically remove a sample, construct the Mahalanobis matrix, and discriminant functions without this sample and then check if this sample is classified correctly. Then the sample returns to the training set and a new sample is removed. The process is continued until every sample has been rotated out once. This gives a more realistic estimate of the true rate of correct classification than that obtained by simply classifying each observation on the discriminant function fitted to the full set of data [31].

TABLE IV
Truth Tables of the VGP-DSP Classification

Method	Classification Result	The lesion is actually melanoma	The lesion is actually dysplastic nevus
Discriminant Analysis using: Irregularity, Thinness Ratio, Average Red, Standard Deviation of Red, I_3, Greatest Diameter and Asymmetry Features	Melanoma (VGP)	13	1
	Dysplastic Nevus (DSP)	0	20
Discriminant Analysis using: Greatest Diameter and the Thinness Ratio as the most significant for discrimination	Melanoma (VGP)	12	2
	Dysplastic Nevus (DSP)	0	20
Neural Networks using four principal components as input	Melanoma (VGP)	13	1
	Dysplastic Nevus (DSP)	0	20
Neural Networks using two principal components as input	Melanoma (VGP)	11	3
	Dysplastic Nevus (DSP)	2	18

Since the values of several other variables also differed between the groups, it is likely that other combinations of variables would be equally successful in discriminating between the two groups. A much larger sample of cases would be necessary to establish clearly which discriminant function gave optimal performance.

The neural networks models also performed very well. Using four principal components as input, the success rate achieved was 97% (93% of VGP and 100% of DSP). This was reduced to 85% correct classification (79% of VGP and 90% of DSP) using only the first two principal components. Using Greatest Diameter and Thinness Ratio for input—that is, the two significant predictors identified above—gave 97% correct classification, exactly as in the discriminant analysis. Both methods, discriminant analysis and neural network, misclassified the same case of malignant melanoma as dysplastic nevus. For each method, a 2 $\times$ 2 truth table was constructed and the results are summarized in Table IV.

Two important measures of the classification method diagnostic value are the sensitivity and specificity indexes, which are defined as

$$\text{Sensitivity} = \frac{\text{True VGP Classification}}{\text{Total number of actual melanomas}} \quad (19)$$

TABLE V
SENSITIVITY AND SPECIFICITY INDEXES OF THE VGP-DSP CLASSIFICATION

Method	Total correct classification	Sensitivity	Specificity
Discriminant Analysis using: Irregularity, Thinness Ratio, Average Red, Standard Deviation of Red, I_3, Greatest Diameter and Asymmetry Features	33/34 or 97%	93%	100%
Discriminant Analysis using: Greatest Diameter and the Thinness Ratio as the most significant for discrimination	32/34 or 94%	86%	100%
Neural Networks using four principal components as input	33/34 or 97%	93%	100%
Neural Networks using two principal components as input	29/34 or 85%	79%	90%

and

$$\text{Specificity} = \frac{\text{True DSP Classification}}{\text{Total number of actual nonmalignant nevus}}. \quad (20)$$

The corresponding indexes were calculated and displayed in Table V.

VII. RGP-DSP COMPARISON

In the preliminary comparison of the RGP and DSP groups, t tests indicated that 9 of the 20 features differed statistically significantly $(P < 0.01)$ between groups. These were Irregularity, Thinness Ratio, Average Red, Average Green, Average Blue, I_1, Average Intensity, Average L, and Greatest Diameter. The stepwise discriminant analysis selected I_1, Greatest Diameter, and Average Saturation. Malignant melanoma was indicated by higher values of the Greatest Diameter (means 156 and 84 for RGP and DSP cases, respectively) and lower values of I_1 (means 33.6 and 61.7, respectively). Values of Average Saturation by themselves were not associated with group membership (means 0.30 and 0.27, respectively), but the sign of this predictor's coefficient in the discriminant function indicated that lower values of Average Saturation, in association with the other two variables selected, indicated malignant melanoma.

This discriminant function classified correctly 97% of the cases (100% of DSP and 93% of RGP). Recalculating the discriminant function without Average Saturation gave much poorer performance (88% correct classification: 90% of DSP and 86% of RGP).

The neural network model achieved 100% correct classification taking four principal components as input and 94% correct (100% of DSP and 86% of RGP) using two components. The cases misclassified by the neural network were not the same case misclassified by the discriminant analysis. Taking as input the three variables that had been selected by the discriminant analysis procedure, the neural network again gave 100% correct classification. The RGP-DSP classification truth tables and the corresponding sensitivity and specificity index results are summarized in Tables VI and VII, respectively.

TABLE VI
TRUTH TABLES OF THE RGP-DSP CLASSIFICATION

Method	Classification Result	The lesion is actually melanoma	The lesion is actually dysplastic nevus
Discriminant Analysis using: I_1, Average Saturation and Greatest Diameter Features	Melanoma (RGP)	13	1
	Dysplastic Nevus (DSP)	0	20
Discriminant Analysis using: I_1, and Greatest Diameter Features as the most significant for discrimination	Melanoma (RGP)	12	2
	Dysplastic Nevus (DSP)	2	18
Neural Networks using four principal components as input	Melanoma (RGP)	14	0
	Dysplastic Nevus (DSP)	0	20
Neural Networks using two principal components as input	Melanoma (RGP)	12	2
	Dysplastic Nevus (DSP)	0	20

TABLE VII
SENSITIVITY AND SPECIFICITY INDEXES OF THE RGP-DSP CLASSIFICATION

Method	Total correct classification	Sensitivity	Specificity
Discriminant Analysis using: I_1, Average Saturation and Greatest Diameter Features	33/34 or 97%	93%	100%
Discriminant Analysis using I_1, and Greatest Diameter Features as the most significant for discrimination	30/34 or 88%	86%	100%
Neural Networks using four principal components as input	34/34 or 100%	100%	100%
Neural Networks using two principal components as input	32/34 or 94%	86%	90%

In similar previous research efforts, Kjoelen *et al.* [51] report an average success rate of 70% in diagnosing melanoma via features extracted by digital images, while Ercal *et al.* using a neural network for the detection of malignant melanoma from color images report a percentage of 86% correct classification [13], [14]. Moreover, Dreiseitl *et al.* [38] have utilized five techniques, namely the k nearest neighbors clustering, logistic regression, artificial neural networks, decision tress, and support

vector machines on the task of classifying pigmented skin lesions as common nevi, dysplastic nevi, or melanoma. The success rates they report fluctuate from 79% to 97%. The results of our research are even slightly better proving the significance of the standardization and reproducibility in image acquisition ensured by the proposed system.

VIII. Conclusion

The technical achievements of recent years in the areas of image acquisition and processing allow the improvement and lower cost of image analysis systems. Such tools may serve as diagnostic adjuncts for medical professionals for the confirmation of a diagnosis, as well as for the training of new dermatologists. In addition, the latest developments in decision support systems give the opportunity of implementing more accurate, faster, and more reliable classification systems. The introduction of diagnostic tools based on intelligent decision support systems is also capable of enhancing the quality of medical care, particularly in areas where a specialized dermatologist is not available. The inability of general physicians to provide high-quality dermatological services leads them to the wrong diagnoses, particularly in evaluating fatal skin diseases such as melanoma [36]. In such cases, an expert system may detect the possibility of a serious skin lesion and warn of the need for early treatment.

A new system for analyzing digital images of skin lesions has been presented in the paper. The system is able to measure objectively, with high repeatability and without presupposing wide experience in image assessment. The adherence to the standardized setup and measurement procedures, which have been presented, may assure the color quality and the repeatability in the images. The high image resolution is achieved through the use of CCDs. Six algorithms for image segmentation and one for image registration were tested for their efficiency using images acquired by the implemented system. Finally, two classification methods were used for the diagnosis of malignant melanoma against dysplastic nevus.

The system features can be summarized as follows:

- acquisition of repeatable and high-quality images, as regards color and resolution;
- noncontact measurements, which prevent the local hematomas that are stimulated through pressure;
- database for storage of the images along with the demographic patient data;
- unsupervised image segmentation and registration of the skin lesions;
- an efficient registration algorithm based on the log-polar transform of the images Fourier spectrum;
- image analysis algorithms for the extraction of measurable features;
- classification schemas for differential diagnosis.

The results from our research are promising for the future. Both the statistical method of discriminant analysis and the application of artificial neural networks led to high percentages of correct allocation of cases to their groups of origin. It is now necessary to examine more patients in order to increase the number of cases, particularly during the classification phase. This will clarify the issue of selecting the most powerful variables for classification and may also enable even better classification if examination of the differences in results between the two methods casts light on why misclassifications can arise.

Acknowledgment

The skin lesion images used for the algorithms efficiency tests were acquired from patients in the General Hospital of Athens G. Gennimatas with the help of the medical personnel of the Department of Plastic Surgery and Dermatology.

References

[1] G. Hansen, E. Sparrow, and J. Kokate, "Wound status evaluation using color image processing," *IEEE Trans. Med. Imag.*, vol. 16, no. 1, pp. 78–86, Feb. 1997.

[2] A. Green, N. Martin, G. McKenzie, J. Pfitzner, F. Quintarelli, and B. W. Thomas *et al.*, "Computer image analysis of pigmented skin lesions," *Melanoma Res.*, vol. 1, pp. 231–236, 1991.

[3] F. Nachbar, W. Stolz, T. Merkle, A. B. Cognetta, T. Vogt, and M. Landthaler *et al.*, "The ABCD rule of dermatoscopy: high prospective value in the diagnosis of doubtful melanocytic skin lesions," *J. Amer. Acad. Dermatol.*, vol. 30, no. 4, pp. 551–559, Apr. 1994.

[4] T. Schindewolf, R. Schiffner, W. Stoltz, R. Albert, W. Abmayr, and H. Harms, "Evaluation of different image acquisition techniques for a computer vision system in the diagnosis of malignant melanoma," *J. Amer. Acad. Dermatol.*, vol. 31, no. 1, pp. 33–41, 1994.

[5] A. Green, N. Martin, J. Pfitzner, M. O'Rourke, and N. Knight, "Computer image analysis in the diagnosis of melanoma," *J. Amer. Acad. Dermatol.*, vol. 31, no. 6, pp. 958–964, Dec. 1994.

[6] S. Seidenari, M. Burroni, G. Dell'Eva, P. Pepe, and B. Belletti, "Computerized evaluation of pigmented skin lesion images recorded by a videomicroscope: Comparison between polarizing mode observation and oil/slide mode observation," *Skin Res. Technol.*, vol. 1, pp. 187–191, 1995.

[7] R. Pompl, W. Bunk, A. Horsch, W. Abmayr, G. Morfill, W. Brauer, and W. Stolz, "Computer vision of melanocytic lesions using MELDOQ," in *Proc. 6th Congress Int. Soc. Skin Imaging*, vol. 5, London, U.K., 1999, p. 150.

[8] H. Ganster, M. Gelautz, A. Pinz, M. Binder, H. Pehamberger, M. Bammer, and J. Krocza, "Initial results of automated melanoma recognition," in *Theory and Applications of Image Analysis II, Selected papers of the 9th SCIA, Scandinavian Conf. Image Analysis*, Singapore, 1995, pp. 343–354.

[9] J. F. Aitken, J. Pfitzner, D. Battistutta, P. K. O'Rourke, A. C. Green, and N. G. Martin, "Reliability of computer image analysis of pigmented skin lesions of Australian adolescents," *Cancer*, vol. 78, no. 2, pp. 252–257, Jul. 1996.

[10] W. V. Stoecker, W. W. Li, and R. H. Moss, "Automatic detection of asymmetry in skin tumors," *Computerized Med. Imag. Graph.*, vol. 16, no. 3, pp. 191–197, May/Jun. 1992.

[11] P. N. Hall, E. Claridge, and J. D. M. Smith, "Computer screening for early detection of melanoma—Is there a future?," *Br. J. Dermatol.*, vol. 132, pp. 325–338, 1995.

[12] T. Ross, H. Handels, J. Kreusch, H. Busche, H. H. Wolf, and S. J. PöpplPoppl, "Automatic classification of skin tumours with high resolution surface profiles," in *Computer Analysis of Images and Patterns Proc. (CAIP '95)*, Berlin, Germany, 1995, LNCS 970, pp. 368–375.

[13] F. Ercal, A. Chawla, W. V. Stoecker, H. C. Lee, and R. H. Moss, "Neural network diagnosis of malignant melanoma from color images," *IEEE Trans. Biomed. Eng.*, vol. 41, no. 9, pp. 837–845, Sep. 1994.

[14] F. Ercal, H. C. Lee, W. V. Stoecker, and R. H. Moss, "Skin cancer classification using hierarchical neural networks and fuzzy systems," *Int. J. Smart Eng. Syst. Design*, vol. 1, pp. 273–289, 1999.

[15] M. Loane, H. Gore, R. Corbet, and K. Steele, "Effect of camera performance on diagnostic accuracy," *J. Telemed. Telecare*, vol. 3, pp. 83–88, 1997.
[16] M. Herbin, F. Bon, and A. Venot *et al.*, "Assessment of healing kinetics through true color image processing," *IEEE Trans. Med. Imag.*, vol. 12, no. 1, pp. 39–43, Mar. 1993.
[17] S. E. Umbaugh, Y. Wei, and M. Zuke, "Feature extraction in image analysis," *IEEE Eng. Med. Biol. Mag.*, vol. 16, no. 4, pp. 62–73, Jul./Aug. 1997.
[18] M. Kjoelen, M. Thompson, S. Umbaugh, R. Moss, and W. Stoecker, "Performance of AI methods in detecting melanoma," *IEEE Eng. Med. Biol. Mag.*, vol. 14, no. 4, pp. 411–416, Jul./Aug. 1995.
[19] M. Nishik and C. Foster, "Analysis of skin erythema using true color images," *IEEE Trans. Med. Imag.*, vol. 16, no. 6, pp. 711–716, Dec. 1997.
[20] T. Lee, V. Ng, R. Gallagher, A. Coldman, and D. McLean, "DullRazor: a software approach to hair removal from images," *Comput. Biol. Med.*, vol. 27, pp. 533–543, 1997.
[21] G. Goldon and G. Nuckols, *Interior Lighting for Designers*, 3rd ed. New York: Wiley, 1995.
[22] *IES Lighting Handbook*, J. E. Kaufman, Ed., Illuminating Eng. Soc. North Amer., 1987.
[23] I. Maglogiannis and D. Kosmopoulos, "A digital image acquisition system for skin lesions," in *SPIE Int. Conf. Medical Imaging*, San Diego, CA, Feb. 15–20, 2003.
[24] D. H. Ballard and C. M. Brown, *Computer Vision*. Englewood Cliffs, NJ: Prentice-Hall, 1982.
[25] S. E. Umbaugh, R. H. Moss, and W. V. Stoecker, "Automatic color segmentation of images with application to detection of variegated coloring in skin tumors," *IEEE Eng. Med. Biol.*, vol. 8, no. 4, pp. 43–52, Dec. 1989.
[26] A. Venot, J. Devaux, M. Herbin, J. Lebruchec, L. Dubertret, Y. Raulo, and J. Roucayrol, "An automated system for the registration and comparison of photographic images in medicine," *IEEE Trans. Med. Imag.*, vol. 7, no. 4, pp. 298–303, Dec. 1988.
[27] C. R. Gonzalez and E. R. Woods, *Digital Image Processing*. Reading, MA: Addison-Wesley, 1995.
[28] A. Cideciyan, "Registration of ocular fundus images, an algorithm using cross-correlation of triple invariant image descriptors," *IEEE Eng. Med. Biol.*, vol. 14, no. 1, pp. 52–58, Jan./Feb. 1995.
[29] Y. I. Ohta, T. Kanade, and T. Sakai, "Color information for region segmentation," *Comput. Graph. Image Process.*, vol. 13, pp. 222–241, 1980.
[30] A. J. Round, W. G. Duller, and P. J. Fish, "Color segmentation for lesion clasification," in *Proc. 19th IEEE/EMBS*, Chicago, IL, 1997, pp. 582–585.
[31] K. V. Mardia, J. T. Kent, and J. M. Bibby, *Multivariate Analysis*. London, U.K.: London Academic Press, 1979.
[32] B. D. Ripley, "Neural networks and related methods for classification," *J. Royal Statistical Soc. B*, vol. 56, no. 3, pp. 409–456, 1994.
[33] C. M. Bishop, *Neural Networks for Pattern Recognition*. London, U.K.: Oxford Clarendon Press, 1995.
[34] S. M. Weiss and C. A. Kulikowski, *Computer Systems That Learn: Classification and Prediction Methods From Statistics, Neural Nets, Machine Learning and Expert Systems*. San Mateo, CA: Morgan Kaufmann, 1991.
[35] J. E. Moody, "The effective number of parameters: an analysis of generalization and regularization in nonlinear learning systems," in *Advances in Neural Information Processing Systems*, J. E. Moody, S. J. Hanson, and R. P. Lippmann, Eds. San Mateo, CA: Morgan Kaufmann, 1992, vol. 4, pp. 847–854.
[36] R. J. Pariser and D. M. Pariser, "Primary care physicians errors in handling cutaneous disorders," *J. Amer. Acad. Dermatol.*, vol. 17, pp. 239–245, 1987.
[37] I. Maglogiannis, C. Caroni, S. Pavlopoulos, V. Karioti, and D. Koutsouris, "Utilizing artificial intelligence for the characterization of dermatological images," in *Proc. 4th Int. Conf. Neural Networks and Expert Systems in Medicine and Healthcare (NNESMED)*, 2001, pp. 362–368.
[38] S. Dreiseitl, L. Ohno-Machado, H. Kittler, S. Vinterbo, H. Billharrt, and M. Binder, "A comparison of machine learning methods for the diagnosis of pigmented skin lesions," *J. Biomed. Informatics*, vol. 34, pp. 28–36, 2001.
[39] Z. Zhang, W. V. Stoecker, and R. H. Moss, "Border detection on digitized skin tumor images," *IEEE Trans. Med. Imag.*, vol. 19, no. 11, pp. 1128–1143, Nov. 2000.
[40] D. H. Chung and G. Sapiro, "Segmenting skin lesions with partial-differential-equations-based image processing algorithms," *IEEE Trans. Med. Imag.*, vol. 19, no. 7, pp. 763–767, Jul. 2000.
[41] H. Ganster, P. Pinz, R. Rohrer, E. Wildling, M. Binder, and H. Kittler, "Automated melanoma recognition," *IEEE Trans. Med. Imag.*, vol. 20, no. 3, pp. 233–239, Mar. 2001.
[42] A. Gutenev, V. Skladnev, and D. Varvel, "Acquisition-time image quality control in digital dermatoscopy of skin lesions," *Comput. Med. Imag. Graph.*, vol. 25, pp. 495–499, 2001.
[43] L. Xu, M. Jackowski, A. Goshtasby, D. Roseman, S. Bines, C. Yu, A. Dhawan, and A. Huntley, "Segmentation of skin cancer images," *Image Vision Comput.*, vol. 17, pp. 65–74, 1999.
[44] P. Schmid-Saugeon, "Symmetry axis computation for almost-symmetrical and asymmetrical objects: Application to pigmented skin lesions," *Med. Image Anal.*, vol. 4, pp. 269–282, 2000.
[45] F. Nachbar, W. Stolz, T. Merkle, A. B. Cognetta, T. Vogt, and M. Landthaler *et al.*, "The ABCD rule of dermatoscopy: High prospective value in the diagnosis of doubtful melanocytic skin lesions," *J. Amer. Acad. Dermatol.*, vol. 30, no. 4, pp. 551–559, Apr. 1994.
[46] C. Grana, G. Pellacani, R. Cucchiara, and S. Seidenari, "A new algorithm for border description of polarized light surface microscopic images of pigmented skin lesions," *IEEE Trans. Med. Imag.*, vol. 22, no. 8, pp. 959–964, 2003.
[47] J. B. A. Maintz and M. A. Viergever, "A survey of medical image registration," *J. Med. Image Anal.*, vol. 2, no. 1, pp. 1–36, 1998.
[48] K. Rohr, H. Stiehl, R. Sprengel, T. Buzug, J. Weese, and M. Kuhn, "Landmark based elastic registration using approximating thin plate splines," *IEEE Trans. Med. Imag.*, vol. 20, no. 6, pp. 526–534, 2001.
[49] W. M. Wells III, P. Viola, H. Atsumi, S. Nakajima, and R. Kikinis, "Multi-modal volume registration by maximization of mutual information," *Med. Image Anal.*, vol. 1, pp. 35–51, 1997.
[50] G. Hance, S. Umbaugh, R. Moss, and W. Stoecker, "Unsupervised color image segmentation with application to skin tumor borders," *IEEE Eng. Med. Biol.*, vol. 15, no. 1, pp. 104–111, Jan./Feb. 1996.
[51] A. Kjoelen, M. Thompson, S. Umbaugh, R. Moss, and W. Stoecker, "Performance of AI methods in detecting melanoma," *IEEE Eng. Med. Biol.*, vol. 14, no. 4, pp. 411–416, Jul./Aug. 1995.
[52] M. Kudo and J. Sklansky, "Comparison of algorithms that select features for pattern classifiers," *Pattern Recognit.*, vol. 33, pp. 25–41, 2000.
[53] S. E. Umbaugh, R. H. Moss, and W. V. Stoecker, "Automatic color segmentation algorithms," *IEEE Eng. Med. Biol.*, vol. 12, no. 3, pp. 75–82, Sep. 1993.
[54] C. Balas, "An imaging colorimeter for noncontact tissue color mapping," *IEEE Trans. Biomed. Eng.*, vol. 44, no. 6, pp. 468–474, Jun. 1997.

I. Maglogiannis (M'00) received the Diploma in electrical and computer engineering and the Ph.D. degree in biomedical engineering from the National Technical University of Athens (NTUA), Greece, in 1996 and 2000, respectively.

From 1996 to 2000, he worked as a Researcher in the Biomedical Engineering Laboratory in NTUA. Since February of 2001, he has been a Lecturer in the Department of Information and Communication Systems Engineering in University of the Aegean. He has been principal investigator in many European and National Research programs in Biomedical Engineering and Health Telematics. He has served on program committees of national and international conferences and he is a reviewer for several scientific journals. His scientific activities include biomedical engineering, image processing, computer vision and multimedia communications. He is the author of over 30 publications in the above areas.

Dr. Maglogiannis is a Member of SPIE and the Hellenic Association of Biomedical Engineering.

S. Pavlopoulos (S'92–M'95) received the degree in electrical engineering from the University of Patras, Greece, in 1987, and the Ph.D. degree in biomedical engineering jointly from Rutgers University and Robert Wood Johnson Medical School, New Brunswick, NJ, in 1992.

He is a Research Associate Professor at the Institute of Communication and Computer Systems, the National Technical University of Athens, Greece. He has published five book chapters, more than 30 journal articles, and more than 45 refereed conference papers. His research interests include medical informatics, telemedicine, medical image and signal processing, and bioinformatics. He has been active in a number of European and National research and development programs in the field of telematics applications in healthcare.

D. Koutsouris (M'96–SM'98) was born in Serres, Greece, in 1955. He received the Diploma in electrical engineering from the University of Patras, Greece, in 1978, the DEA degree in biomechanics from Rene Descartes University of Paris, France, in 1979, the Doctorat in general biology and medicine from the University of Paris III, France, in 1982, and the Doctorat d' Etat in biomedical engineering and biophysics from the University of Paris V, France, in 1984.

Since 1986, he has been a Associate Researcher with University of Southern California (USC), Los Angeles, Rene Descartes, Paris, France, and Associate Professor in the Department of Electrical and Computer Engineering, National Technical University of Athens, Greece. He is currently Professor and Chairman of the Department of Electrical and Computer Engineering, National Technical University of Athens and head of the Biomedical Engineering Laboratory. He has published over 100 research articles and book chapters and more than 150 conference communications. Recently, he has also been elected President of the Greek Society of Biomedical Technology. He has been principal investigator in many European and national research programs, especially in the field of telematics applications in healthcare.